JOURNAL OF GEOPHYSICAL RESEARCH, VOL. 99, NO. B8, PAGES 15,761–15,775, AUGUST 10, 1994

# The influence of room temperature deformation on porosity and permeability in calcite aggregates

Shuqing Zhang,[1] Stephen F. Cox, and Mervyn S. Paterson

**Research School of Earth Sciences, Australian National University, Canberra**

**Abstract.** Changes in permeability and porosity during shortening deformation of Carrara marble and hot-pressed calcite aggregates were measured under high pressure at room temperature using argon as pore fluid. At effective pressures of 30 and 50 MPa, the permeability of Carrara marble increased by up to 2 orders of magnitude with less than 2% strain during which the connected porosity increased by only 0.005. The permeability increased more slowly with further strain up to 18%, during which the connected porosity increased by a further 0.05 to 0.06. At effective pressures of 100 MPa to 200 MPa, these effects were much less marked. In hot-pressed calcite aggregates, deformed at an effective pressure of 50 MPa, the permeability increased by about 2 orders of magnitude after about 12% strain and an increase in connected porosity of about 0.03. Microstructural studies indicate that, in the coarse-grained Carrara marble specimens, both transgranular and grain boundary cracks are present after room temperature deformation. For a given strain, the average length and the linear density of transgranular cracks decrease with increasing effective pressure. In fine-grained, hot-pressed calcite aggregates, dilatancy is mainly due to opening of grain boundary cracks. The very marked increase in permeability with small strain at low effective pressure can be correlated with the proliferation of connected microcracks of relatively large apertures, deduced on the basis of theoretical models.

## Introduction

In many regional metamorphic terranes, mineral-fluid equilibria and stable isotope studies, as well as mass transfer associated with foliation development, indicate widespread fluid infiltration and fluid-rock interactions during metamorphism and regional deformation [e.g., *Etheridge et al.*, 1983, 1984; *Wood and Walther*, 1986]. Fluid migration can involve localized flow along macroscopic fracture networks, especially within active faults and shear zones [e.g., *Kerrich*, 1986; *Sibson et al.*, 1988; *McCaig*, 1988; *Moore and Vrolijk*, 1992] or more pervasive percolation through grain edge channels and grain-scale microcracks [*Etheridge et al.*, 1983; *Vaughan et al.*, 1986; *Brantley et al.*, 1990; *Lee et al.*, 1991; *Brantley*, 1992]. Deformation-induced microcrack permeability appears to be an important factor influencing pervasive fluid flow during crustal deformation [*Beach*, 1980; *Etheridge et al.*, 1984; *Smith and Evans*, 1984; *Rutter and Brodie*, 1985; *Cox et al.*, 1987; *Cox and Etheridge*, 1989; *Brantley*, 1992].

In this study we examine the evolution of connected microcrack porosity and permeability during macroscopically ductile deformation of calcite rocks at room temperature. Previous work on the deformation of calcite rocks at room temperature has dealt primarily with the mechanical and volumetric behavior [*Heard*, 1963; *Scholz*, 1968; *Edmond and Paterson*, 1972; *Rutter*, 1974; *Olsson and Peng*, 1976; *Fischer and Paterson*, 1989; *Fredrich et al.*, 1989]. These experiments have demonstrated that a small amount of microcrack porosity can develop even when deformation is achieved predominantly by crystal plasticity, and that the development of microcrack porosity is enhanced at low effective pressures. It has also been shown that microcrack porosity resulting from deformation can lead to a significant permeability increase and therefore enhance fluid flow [*Peach*, 1991; *Fischer and Paterson*, 1992]. In order to explore this question further, we have made simultaneous measurements of permeability and connected porosity during ductile deformation of Carrara marble and synthetic calcite aggregates. In this paper we present experimental results on the effects of strain on connected porosity, permeability and storativity (storage capacity per unit volume), and we analyze relationships between these quantities. The evolution of microcrack geometry is then described and, finally, the influence of effective pressure and crack geometry on the relationships between permeability and connected porosity are discussed. We demonstrate the importance of deformation in dramatically enhancing fluid transport properties of rocks at high pressures, even when microfracturing contributes only a small proportion of the total strain.

## Starting Materials and Experimental Procedures

### Starting Materials

Carrara marble and synthetic calcite aggregates were used in the present study. Carrara marble has an average grain size of 160 μm and a total porosity of 0.01. The grains are equant shaped with sutured boundaries and a few twin lamellae. The Carrara marble specimens were 21 mm in length and 10.08 mm in diameter. The synthetic calcite specimens (designated HP-I) were fabricated by hot-pressing ground Wombeyan marble powder at 1073 K and 200 MPa for 3 1/2 hours. The HP-I

[1]Now at Department of Geology and Geophysics, University of Minnesota at Minneapolis.

Copyright 1994 by the American Geophysical Union.

Paper number 94JB00647.
0148-0227/94/94JB-00647$05.00

specimens had a diameter of 9.25 mm, a length of 18 to 20 mm, a very uniform grain size of about 18 μm, and a total porosity of 0.015.

## Experimental Procedures and Techniques

Deformation experiments were performed in an internally-heated, argon confining medium, high-pressure apparatus [*Paterson*, 1970]. The specimens were deformed at room temperature, confining pressures of 200 MPa or 300 MPa, argon pore pressure of 100 MPa to 270 MPa, and a nominal strain rate of $1.2 \times 10^{-4}$ s$^{-1}$. Stress differences were calculated assuming a uniform increase in specimen cross-section with strain at constant volume.

**Pore fluid system and specimen assembly.** The pore fluid system includes an upstream "reservoir," the specimen, and a downstream "reservoir" as described by *Zhang et al.* [this issue]. The upstream "reservoir" consists of the hollow piston, connecting tube, pressure transducer, and volumometer and has a volume about 1400 to 2000 mm$^3$. The volumometer is a cylinder and piston device, driven by a printed armature DC servo-motor through reduction gears. The piston displacement is measured with a DC-LVDT. The downstream "reservoir" consists of the hollow piston, connecting tube and a pressure transducer and has a volume of about 800 mm$^2$. The minimum detectable changes in pore volume and porosity depend on the response of the servo-system and are given in Table 1.

The specimen assembly is shown in Figure 1. In the case of the Carrara marble, a Teflon sleeve was inserted between the iron jacket and the specimen to prevent fluid flow along the specimen/jacket interface. In tests with an impermeable specimen at effective pressures higher than 15 MPa, no argon pore fluid flowed along the specimen-Teflon-iron interfaces. In the case of the synthetic calcite aggregate, a tight seal was formed between the specimen and its iron jacket during hot isostatic pressing; the deformation was carried out immediately after hot pressing, while still at high pressure.

**Procedures and techniques for measuring connected porosity.** In nine experiments (Table 2), performed initially to analyze the microcrack geometry and measure the evolution of connected porosity with strain, the downstream reservoir was blocked off. In each run, pore fluid pressure and confining pressure were first simultaneously raised to the required values. The pore pressure system was then isolated and confining pressure was further raised to 200 MPa. After pore pressure and confining pressure were stabilized, the axial load was applied and the deformation experiment was carried out.

**Table 1.** The Resolution of the Volumometer in Terms of Volume and Porosity

| Pore Pressure MPa | Minimum Detectable Volume Change, mm$^3$ | | Minimum Detectable Porosity Change* | |
|---|---|---|---|---|
| | Without | With | Without | With |
| 50 | 4.9 | 9.55 | 0.0039 | 0.0061 |
| 100 | 1.9 | 3.50 | 0.0013 | 0.0022 |
| 150 | 1.1 | 1.98 | 0.0007 | 0.0013 |
| 200 | 0.7 | 1.37 | 0.0004 | 0.0009 |
| 250 | 0.5 | 1.00 | 0.0003 | 0.0006 |
| 275 | 0.5 | 0.88 | 0.0003 | 0.0006 |

Without downstream reservoir and with downstream reservoir connected.

*Assuming a specimen volume of 1570 mm$^3$.

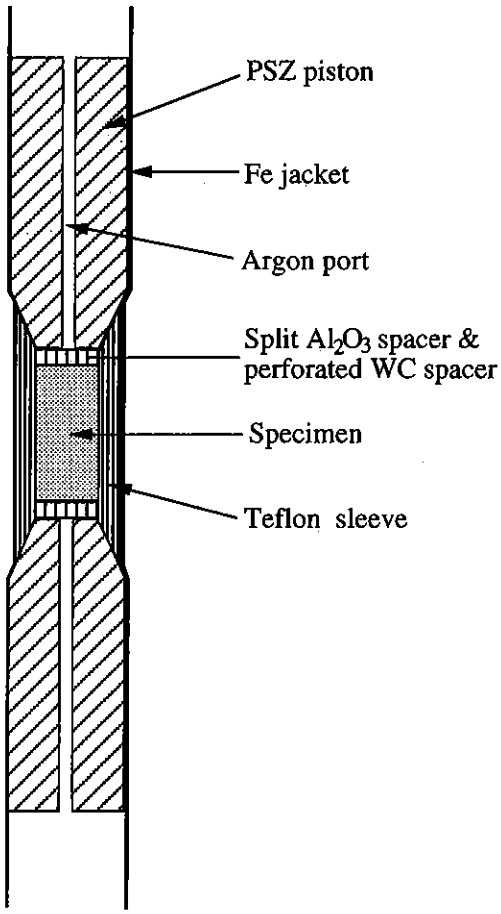


**Figure 1.** Details of specimen assembly. A Teflon sleeve was put between the specimen and an iron jacket to prevent fluid flow along the specimen/jacket interface.

The servo-controlled volumometer measured the volume of fluid moving in or out of the specimen during deformation, as in the study of *Fischer and Paterson* [1989], with a view to monitor changes in connected (open) porosity. However, these measurements must be interpreted with care because, apart from reflecting directly the changes in connected porosity $\phi_c$, they may also be affected by the establishment of new connection into previously closed porosity. A response due to the latter effect will be registered if the previous fluid pressure in the newly opened pores is different from that in the volumometer system, resulting in fluid movement when the new connection is made. Because of this possible complication, we shall refer to the relative volume changes registered with the volumometer as " apparent connected porosity changes," designated as $\Delta\phi_v$ [cf. *Zhang et al.*, this issue]. Thus $\Delta\phi_v = \Delta\phi_c + \delta$, where $\delta$ is the effect of equalizing the fluid pressure in the newly-opened pores with the imposed pore pressure and may be positive or negative. The values of $\Delta\phi_v$ will, however, reflect the dilatation $\Delta\phi_c$ in the specimen to a fairly good approximation because of the relatively small amount of total initial porosity (0.01 to 0.015, and hence even smaller initial closed porosity) and of the likelihood that the new microcrack porosity will remain connected throughout the room-temperature experiments.

**Table 2.** Connected Porosity Experiments

| Run | Material | $P_c$ MPa | $P_f$ MPa | Strain % | $\Delta\phi_v$ | $N^{\#}$ | $a^{*}$ mm | $n^{+}$ 1/mm |
|---|---|---|---|---|---|---|---|---|
| 3835 | Carrara | 200 | 170 | 2.5 | 0.005 | 83 | 131±8 | 18±2 |
| 3836 | Carrara | 200 | 170 | 15.0 | 0.060 | 71 | 186±9 | 25±4 |
| 3851 | Carrara | 200 | 150 | 4.0 | 0.023 | 290 | 83±3 | 7±2 |
| 3838 | Carrara | 200 | 150 | 12.0 | 0.042 | 326 | 100±3 | 15±2 |
| 3891 | Carrara | 200 | 150 | 15.0 | 0.055 | 445 | 101±3 | 20±2 |
| 3897 | Carrara | 300 | 200 | 7.6 | 0.030 | 225 | 98±4 | 11±2 |
| 3901 | Carrara | 300 | 100 | 17.2 | 0.014 | 240 | 61±3 | 6±1 |
| 3826 | HP-I | 200 | 180 | 8.2 | 0.055 | | | |
| 3840 | HP-I | 200 | 150 | 12.3 | 0.007 | | | |
| 3815 | HP-I | 200 | 100 | 8.7 | 0.000 | | | |

# The number of observations.
* The average length $a$ for transgranular cracks; standard error is also given.
+ The abundance $n$ of transgranular cracks within the line length of 15 mm to 25 mm.

**Procedures and techniques for measuring permeability and storativity.** In further deformation experiments on five Carrara marble and one HP-I calcite specimens (Table 3), the permeability ($k$), storativity ($\beta_c$), and changes in apparent connected porosity ($\Delta\phi_v$) were simultaneously measured. In these experiments, the downstream "reservoir" was connected and the same pressurizing procedure was followed as before. After the pore pressure in the specimen and upstream and downstream reservoirs had equilibrated, an initial permeability measurement was conducted on the intact rock specimen. Then, deformation was carried out incrementally, being halted for each permeability determination (Figure 2).

The permeability ($k$) and "storativity" ($\beta_c$) were determined by the "oscillating pore pressure" technique [*Fischer and Paterson*, 1988, 1992; *Kranz et al.*, 1990; *Fischer*, 1992]. This technique is based on the measurement of the amplitude attenuation ($\alpha$) and phase retardation ($\delta$) of a sinusoidal pore pressure oscillation as it propagates through the specimen. The oscillation amplitude used was between 1 MPa and 12 MPa and oscillation period between 16 s and 8112 s.

Based on the analysis of the experimental constraints, the range of permeability measurable in our system is estimated to be from $10^{-21}$ to $10^{-16}$ m$^2$ and storativity from $10^{-11.5}$ to $10^{-7.5}$ Pa$^{-1}$. The reproducibility of permeability and storativity is usually within a factor of 1.2 and 5, respectively. However, the precision varies considerably within the field of $\alpha$ and $\delta$ and in some cases, $\beta_c$ can change 1 to 2 orders of magnitude with less than 1% variation in $\alpha$ and $\delta$ and therefore can not be precisely determined (see *Zhang et al.* [this issue] for discussion).

Due to the frictional constraint at the contact between the specimen and the loading pistons, a conical, less deformed and less permeable region is usually present at each end of a deformed specimen. The maximum depth of this region is about 0.75 - 1 mm in Carrara marble and 0.5 mm in hot-pressed calcite. On the assumption that the end regions have the same permeability as the undeformed specimens, their presence is estimated to result in underevaluation of the permeability by a factor not exceeding 3 or $10^{0.5}$.

As shown in Figure 2, stress relaxation occurred immediately after the driving ram was halted for a permeability determination. Because of the stress relaxation and the slow re-establishment of pore pressure equilibrium in the downstream reservoir, a time delay was usually needed before a pore pressure oscillation test was performed.

## Experimental Results

### Measurements

**Carrara marble.** Five Carrara marble specimens were deformed in compression at room temperature and effective pressures of 30, 50, 100, 150, and 200 MPa (Table 3 and Figure 3a). The serrations in the strain-stress curves represent the strain relaxation during halts for permeability measurements, mentioned above. At higher effective pressure, the flow stresses and magnitudes of stress relaxation are larger. The stress decreased exponentially with time and recovered rapidly at the beginning of the following increment of deformation.

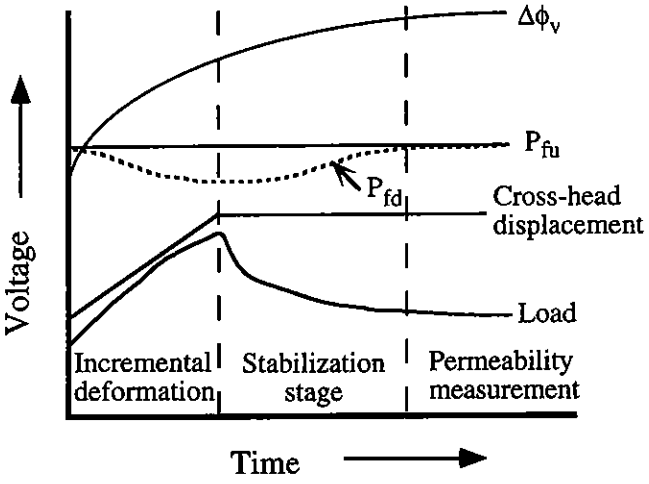


**Figure 2.** Schematic diagram of experimental procedures for the measurements of permeability, storativity, and the change in connected porosity in incremental deformation. Deformation is halted after each increment of strain. Because of the stress relaxation and time delay in measuring the increase in connected porosity, a stabilization period is needed before a permeability measurement is conducted. $P_{fu}$ and $P_{fd}$ are the pore pressures in the upstream and downstream reservoir, respectively.

**Table 3.** Permeability and Storativity Experiments

| $P_f$ MPa | Strain % | Stress MPa | Period s | $P_a$ MPa | α | δ rad | γ | ψ | log $k$ $m^2$ | log $\beta_c$ $Pa^{-1}$ | $\Delta\phi_v$ | $x$ nm | $\beta_c/\phi_c\beta_f$ | $a/c$ |
|---|---|---|---|---|---|---|---|---|---|---|---|---|---|---|
| *Experiment 3898, Carrara Marble, Confining Pressure = 300 MPa, $L_0$ = 18.85 mm, $A_0$ = 78.54 mm$^3$* | | | | | | | | | | | | | | |
| 250 | 0.0 | 0 | 790 | 4.4 | 0.2719 | 1.2735 | **** | **** | -19.26 | **** | 0.0000 | 164 | | |
| 250 | 0.0 | 0 | 395 | 4.2 | 0.1167 | 1.4129 | **** | **** | -19.37 | **** | 0.0000 | 145 | | |
| 250 | 1.1 | 182 | 790 | 4.4 | 0.3236 | 1.2338 | **** | **** | -19.21 | **** | 0.0000 | 174 | | |
| 250 | 1.9 | 238 | 395 | 4.4 | 0.6462 | 0.8638 | **** | **** | -18.52 | **** | 0.0029 | 244 | | |
| 250 | 1.9 | 227 | 100 | 2.8 | 0.2035 | 1.3260 | **** | **** | -18.53 | **** | 0.0029 | 241 | | |
| 250 | 2.8 | 255 | 100 | 2.8 | 0.3437 | 1.1931 | **** | **** | -18.29 | **** | 0.0088 | 182 | | |
| 250 | 2.8 | 255 | 50 | 2.2 | 0.1650 | 1.4108 | 171.900 | 0.131 | -18.32 | -11.26 | 0.0088 | 176 | 0.37 | |
| 250 | 4.0 | 269 | 50 | 2.1 | 0.2601 | 1.3158 | 75.992 | 0.155 | -18.13 | -10.90 | 0.0164 | 141 | 0.55 | |
| 250 | 4.0 | 269 | 100 | 2.8 | 0.4654 | 1.1035 | 18.229 | 0.228 | -18.13 | -10.28 | 0.0164 | 141 | 2.31 | |
| 250 | 5.9 | 285 | 100 | 2.8 | 0.5511 | 0.9876 | 500.600 | 0.039 | -18.04 | -11.71 | 0.0287 | 99 | 0.05 | |
| 250 | 5.9 | 285 | 50 | 2.2 | 0.3192 | 1.2036 | **** | **** | -18.05 | **** | 0.0287 | 98 | | |
| 250 | 8.0 | 288 | 50 | 2.1 | 0.3687 | 1.2019 | 47.794 | 0.161 | -17.98 | -10.68 | 0.0417 | 77 | 0.42 | |
| 250 | 8.0 | 288 | 100 | 2.8 | 0.5976 | 0.9334 | 72.343 | 0.096 | -18.00 | -10.86 | 0.0417 | 75 | 0.28 | |
| 250 | 10.1 | 288 | 50 | 2.1 | 0.4196 | 1.1841 | 7.232 | 0.377 | -17.91 | -9.85 | 0.0546 | 65 | 2.25 | 102 |
| 250 | 13.1 | 288 | 50 | 2.1 | 0.3624 | 1.2371 | 11.070 | 0.336 | -18.01 | -10.02 | 0.0656 | 49 | 1.27 | |
| 250 | 15.7 | 288 | 50 | 2.2 | 0.3254 | 1.3172 | 5.723 | 0.487 | -18.06 | -9.72 | 0.0736 | 42 | 2.29 | 105 |
| 250 | 15.9 | 288 | 50 | 2.1 | 0.4166 | 1.2043 | 5.219 | 0.439 | -17.93 | -9.68 | 0.0736 | 48 | 2.49 | 122 |
| *Experiment 3899, Carrara Marble, Confining Pressure = 300 MPa, $L_0$ = 18.80 mm, $A_0$ = 78.54 mm$^3$* | | | | | | | | | | | | | | |
| 200 | 0.0 | 0 | 3040 | 9.0 | 0.1674 | 1.3533 | **** | **** | -19.96 | **** | 0.0000 | 92 | | |
| 200 | 3.9 | 290 | 1575 | 4.5 | 0.2635 | 1.3037 | **** | **** | -19.34 | **** | 0.0046 | 87 | | |
| 200 | 3.9 | 290 | 525 | 4.4 | 0.0801 | 1.5287 | 58.820 | 0.338 | -19.39 | -10.65 | 0.0046 | 82 | 1.83 | |
| 200 | 5.8 | 326 | 525 | 4.5 | 0.0929 | 1.5160 | 45.676 | 0.339 | -19.33 | -10.57 | 0.0134 | 43 | 1.09 | |
| 200 | 8.6 | 349 | 525 | 4.5 | 0.1092 | 1.5012 | 37.379 | 0.349 | -19.28 | -10.47 | 0.0218 | 31 | 0.93 | |
| 200 | 11.2 | 371 | 525 | 4.5 | 0.1149 | 1.4851 | 16.795 | 0.442 | -19.15 | -10.11 | 0.0297 | 28 | 1.62 | |
| 200 | 14.7 | 385 | 525 | 4.5 | 0.2322 | 1.4009 | 10.303 | 0.444 | -18.96 | -9.88 | 0.0407 | 26 | 2.08 | 117 |
| 200 | 17.0 | 397 | 525 | 4.5 | 0.3166 | 1.2939 | 10.587 | 0.368 | -18.82 | -9.88 | 0.0458 | 27 | 1.83 | |
| *Experiment 3900, Carrara Marble, Confining Pressure = 300 MPa, $L_0$ = 18.81 mm, $A_0$ = 78.54 mm$^3$* | | | | | | | | | | | | | | |
| 150 | 0.0 | 0 | 5065 | 9.0 | 0.0763 | 1.5019 | 290.830 | 0.150 | -20.30 | -11.23 | 0.0000 | 83 | 0.94 | |
| 150 | 3.9 | 299 | 3040 | 11.6 | 0.0691 | 1.5503 | 48.825 | 0.383 | -20.14 | -10.45 | 0.0028 | 51 | 2.92 | 306 |
| 150 | 7.5 | 372 | 3040 | 11.5 | 0.0789 | 1.4114 | **** | **** | -20.10 | **** | 0.0097 | 25 | | |
| 150 | 11.6 | 428 | 3040 | 11.5 | 0.2916 | 1.2648 | **** | **** | -19.54 | **** | 0.0186 | 28 | | |
| 150 | 14.5 | 422 | 790 | 4.5 | 0.1639 | 1.4171 | 91.165 | 0.182 | -19.23 | -10.67 | 0.0253 | 30 | 0.36 | |
| 150 | 18.0 | 450 | 525 | 2.9 | 0.1331 | 1.4096 | **** | **** | -19.16 | **** | 0.0303 | 28 | | |
| *Experiment 3901, Carrara marble, Confining Pressure = 300 MPa, $L_0$ = 18.65 mm, $A_0$ = 78.54 mm$^3$* | | | | | | | | | | | | | | |
| 100 | 0.0 | 0 | 8110 | 9.1 | 0.0513 | 1.4285 | **** | **** | -20.58 | **** | 0.0000 | 90 | | |
| 100 | 9.9 | 406 | 8110 | 11.7 | 0.0251 | 1.5594 | 123.100 | 0.401 | -20.93 | -10.60 | 0.0045 | 19 | 1.03 | |
| 100 | 17.2 | 518 | 2025 | 9.0 | 0.1671 | 1.4615 | 16.114 | 0.424 | -19.53 | -9.68 | 0.0147 | 30 | 3.30 | 660 |

**Table 3.** continued

| $P_f$ MPa | Strain % | Stress MPa | Period s | $P_a$ MPa | α | δ rad | γ | ψ | log $k$ $m^2$ | log $\beta_c$ $Pa^{-1}$ | $\Delta\phi_v$ | $x$ nm | $\beta_c/\phi_c\beta_f$ | $a/c$ |
|---|---|---|---|---|---|---|---|---|---|---|---|---|---|---|
| *Experiment 3902, Carrara Marble, Confining Pressure = 300 MPa, $L_0$ = 19.10 mm, $A_0$ = 78.54 $mm^3$* | | | | | | | | | | | | | | |
| 270 | 0.0 | 0 | 790 | 5.7 | 0.0662 | 1.4809 | **** | **** | -19.71 | **** | 0.0000 | 98 | | |
| 270 | 1.9 | 162 | 100 | 4.2 | 0.4919 | 1.0647 | 36.134 | 0.150 | -17.85 | -10.65 | 0.0058 | 387 | 2.12 | 84 |
| 270 | 1.9 | 162 | 100 | 2.8 | 0.4894 | 1.0730 | 21.277 | 0.202 | -17.88 | -10.42 | 0.0058 | 373 | 3.61 | 195 |
| 270 | 1.9 | 162 | 50 | 2.3 | 0.2806 | 1.3135 | 20.322 | 0.289 | -17.88 | -10.40 | 0.0058 | 373 | 3.78 | 208 |
| 270 | 2.6 | 185 | 50 | 2.3 | 0.4049 | 1.1678 | 26.346 | 0.205 | -17.70 | -10.51 | 0.0112 | 305 | 1.95 | |
| 270 | 2.6 | 185 | 25 | 1.9 | 0.2099 | 1.4235 | 11.486 | 0.444 | -17.70 | -10.15 | 0.0112 | 305 | 4.47 | 259 |
| 270 | 3.6 | 187 | 25 | 1.8 | 0.3813 | 1.2408 | 6.526 | 0.420 | -17.41 | -9.90 | 0.0201 | 275 | 5.13 | 308 |
| 270 | 3.6 | 185 | 50 | 1.9 | 0.6426 | 0.9122 | 4.515 | 0.349 | -17.40 | -9.74 | 0.0201 | 278 | 7.36 | 475 |
| 270 | 4.7 | 193 | 25 | 1.7 | 0.5511 | 1.0525 | 3.308 | 0.455 | -17.19 | -9.60 | 0.0306 | 250 | 7.13 | 457 |
| 270 | 4.7 | 193 | 15 | 1.1 | 0.3650 | 1.2276 | 13.477 | 0.302 | -17.25 | -10.21 | 0.0306 | 233 | 1.77 | |
| 270 | 6.0 | 190 | 15 | 1.0 | 0.4840 | 1.1148 | 3.132 | 0.505 | -17.07 | -9.57 | 0.0424 | 215 | 5.81 | 359 |
| 270 | 6.0 | 190 | 25 | 1.0 | 0.6785 | 0.8855 | 2.488 | 0.438 | -17.04 | -9.47 | 0.0424 | 223 | 7.36 | 474 |
| 270 | 7.6 | 196 | 25 | 1.2 | 0.7052 | 0.8697 | 1.524 | 0.518 | -16.98 | -9.25 | 0.0536 | 193 | 9.86 | 660 |
| 270 | 7.6 | 196 | 15 | 1.0 | 0.4954 | 1.1236 | 3.572 | 0.469 | -17.07 | -9.62 | 0.0536 | 174 | 4.16 | 236 |
| *Experiment 3893, HP-1, Confining Pressure = 200 MPa, $L_0$ = 18.60 mm, $A_0$ = 69.67 $mm^3$* | | | | | | | | | | | | | | |
| 150 | 0.0 | 0 | 4050 | 2.9 | 0.0948 | 1.4129 | **** | **** | -20.05 | **** | 0.0000 | | | |
| 150 | 5.8 | 360 | 200 | 2.9 | 0.1364 | 1.5168 | 13.382 | 0.502 | -18.58 | -9.81 | 0.0102 | 168 | 6.56 | 878 |
| 150 | 5.8 | 360 | 395 | 2.9 | 0.2852 | 1.2798 | **** | **** | -18.56 | **** | 0.0102 | 172 | | |
| 150 | 8.6 | 380 | 200 | 2.9 | 0.1978 | 1.3009 | **** | **** | -18.44 | **** | 0.0201 | 102 | | |
| 150 | 8.6 | 380 | 395 | 3.0 | 0.3829 | 1.1884 | 36.258 | 0.177 | -18.42 | -10.23 | 0.0201 | 105 | 1.34 | |
| 150 | 10.6 | 383 | 200 | 2.9 | 0.1986 | 1.3581 | **** | **** | -18.45 | **** | 0.0267 | 77 | | |
| 150 | 10.6 | 383 | 395 | 3.0 | 0.3697 | 1.1841 | **** | **** | -18.46 | **** | 0.0267 | 76 | | |
| 150 | 12.2 | 375 | 200 | 3.0 | 0.4300 | 1.1212 | **** | **** | -18.08 | **** | 0.0315 | 100 | | |
| 150 | 12.2 | 375 | 100 | 3.0 | 0.2402 | 1.3531 | 25.519 | 0.274 | -18.06 | -10.06 | 0.0315 | 102 | 1.28 | |
| 150 | 12.2 | 375 | 395 | 3.0 | 0.7115 | 0.7831 | 39.525 | 0.108 | -18.05 | -10.25 | 0.0315 | 103 | 0.83 | |

$P_a$ is the amplitude of pore pressure oscillation, α is the attenuation factor, δ is the phase shift, $k$ is the permeability, $\beta_c$ is the storativity, $\beta_f$ is fluid (argon) compressiblity, $\Delta\phi_v$ is the apparent connected porosity, $\phi_c$ is connected porosity, $x$ is the model crack aperture, $a/c$ is the model crack aspect ratio. Asterisks indicate where storativity could not be precisely determined.

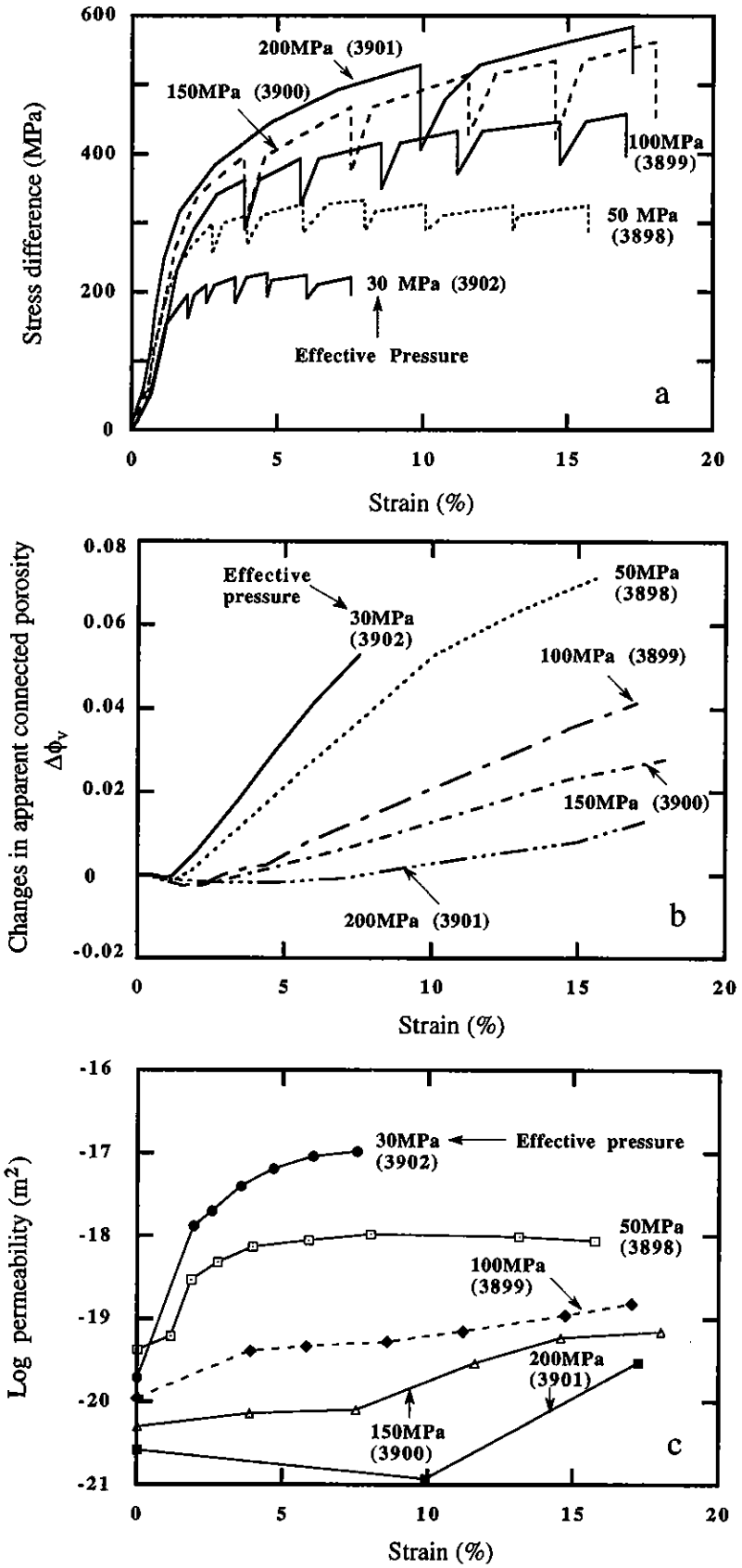


**Figure 3.** Carrara marble deformed at room temperature and various effective pressures as indicated. Run numbers are shown in parentheses. (a) Stress versus strain curves. (b) Changes in apparent connected porosity versus strain. (c) Permeability versus strain. (d) Storativity vs strain. The number on each data point of run 3902 is the pore pressure oscillation period. The solid lines are the best linear fit to the experimental data at effective pressures of 30, 50, and 100 MPa.

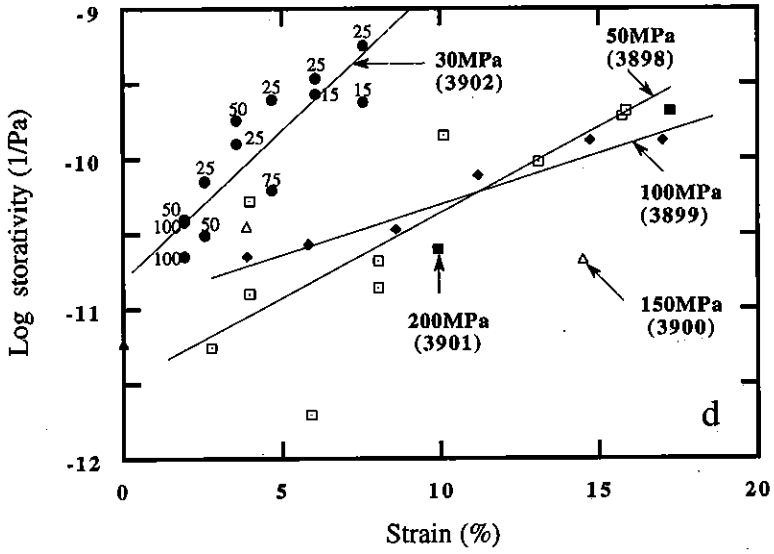


**Figure 3.** (continued)

The changes in apparent connected porosity ($\Delta\phi_v$) with strain are shown in Figure 3b. At effective pressures of 30 MPa and 50 MPa, where a slight strain softening developed (Figure 3a), a large increase in porosity occurred at low strains. At higher effective pressures, where strain hardening occurred throughout the experiment, a less marked increase in porosity had occurred by strains as high as 10 - 15%. The $\Delta\phi_v$ - strain curves at strains from 2% to 10% are approximately linear and the slopes decrease with increasing effective pressure. The slopes also decrease with increasing strain at low effective pressures. Our experimental results are consistent with those of *Fischer and Paterson* [1989] in terms of yield stress and the stress at which a positive change in connected porosity starts. At effective pressures of 30 and 50 MPa, these two stresses approximately coincide, suggesting that microcracking is involved in the yielding. At higher effective pressures, the dilatation commences after yielding.

Permeability results (Table 3) are plotted as a function of strain in Figure 3c. The trends are strongly influenced by the effective pressure. Unlike the porosity, the permeability does not increase at a uniform rate with increasing strain. At effective pressures of 30 MPa and 50 MPa, the permeability jumped about 1 to 2 orders of magnitude during the initial 2% shortening. It then gradually increased by about a half to 1 order of magnitude with further strain up to about 8% and subsequently remained approximately constant up to 16% strain. At an effective pressure of 100 MPa, an initial 4% shortening led to a permeability increase of about half an order of magnitude, after which the permeability increased slowly with increasing strain. At effective pressures of 150 MPa and 200 MPa, the permeability changed only slightly with shortening up to 8% to 10% and then increased about 1 to 1.5 orders of magnitude with further strain to about 15%.

The storativity ($\beta_c$) measurements (Table 3) are plotted as a function of strain in Figure 3d. In general, $\beta_c$ increases with increasing strain and the slope of log $\beta_c$ against strain increases with decreasing effective pressure. Some of the measurements suggest dependence on the oscillation period [cf. *Fischer and Paterson*, 1992; *Zhang et al.*, this issue], but the sense of the effect is inconsistent and any real effect may be obscured by the scatter.

**HP-I synthetic calcite aggregates.** Three hot-pressed calcite aggregate specimens were deformed by shortening at room temperature and effective pressures of 20, 50, and 100 MPa, respectively, without interruptions for permeability measurements (Figure 4a). With increasing effective pressure, HP-I displays a transition from strain softening associated with localized shear zones, to strain hardening and more distributed deformation. Samples deformed at low effective pressures exhibited an earlier and larger increase in apparent connected porosity than at high effective pressure (Figure 4b). HP-I is significantly stronger than Carrara marble at a given effective pressure, possibly due to its smaller grain size [cf. *Fredrich et al.*, 1990].

The permeability and storativity were measured at intervals during progressive deformation of one HP-I calcite specimen at an effective pressure of 50 MPa (Table 3 and Figure 4c). The permeability increased with strain, but the corresponding $\beta_c$ data were too scattered to show any trend.

## Microstructures

Microcracks were observed to have been developed subparallel to the maximum compression direction in all the deformed specimens. The length and abundance of the cracks have been measured on polished surfaces cut parallel to the maximum compression direction, counting the number of cracks along lines normal to the maximum compression direction. Transgranular cracks at high angles (>45°) to the maximum compression direction and grain boundary cracks were excluded in the measurements because they could have formed during either decompression or be significantly modified by decompression. It is known that significant non-elastic deformation which includes microcracking may occur during pressure release after deformation at high pressure [*Paterson*, 1963; *Edmond and Paterson*, 1972]. However, the measurements of *Edmond and Paterson* [1972] indicate that for tests at pressures up to 200 MPa, the dilatation during the deformation is much larger than that during pressure release. Therefore we expect that, in the present experiments, the major part of the microcracking observed microscopically has occurred during the deformation and that during pressure release the pattern of microcracking will not have been

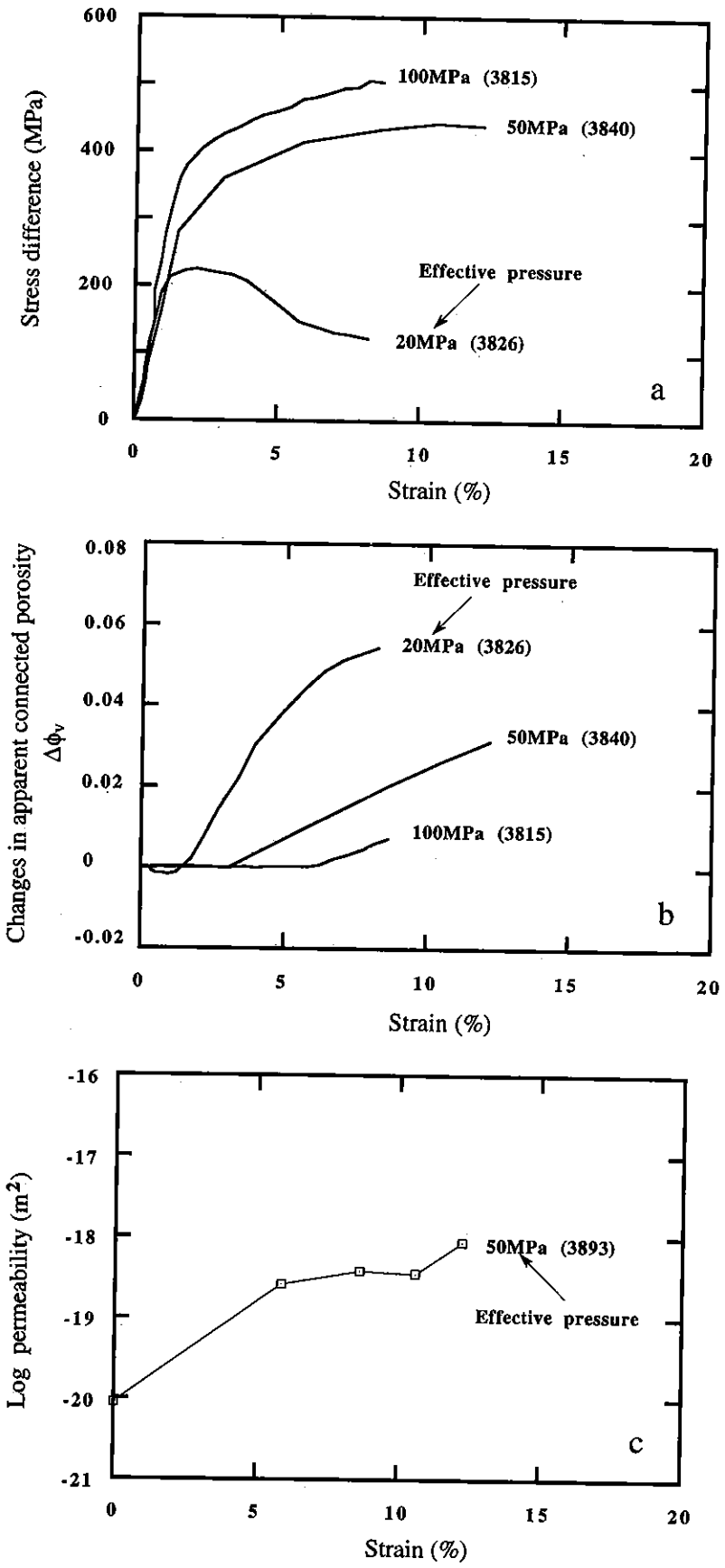


**Figure 4.** HP-I synthetic calcite aggregates deformed at room temperature and effective pressures of 20, 50, and 100 MPa. The specimens were previously hot-pressed at an effective pressure of 200 MPa and 1073 K for 3.5 hours. Run numbers are shown in parenthese. (a) Stress versus strain. (b) Changes in apparent connected porosity versus strain. (c) Permeability versus strain.

changed in a major way, although cracks of some orientations may have become more emphasized than others.

**Carrara marble.** Intragranular cracks are rare in the undeformed Carrara marble (Figure 5a). The length ($a$) and the abundance ($n$) of the subaxial transgranular microcracks were measured in the central parts of seven of the deformed specimens (Table 2).

At an effective confining pressure of 30 MPa, abundant microcracks are already present throughout the specimen at 2.5% strain, except adjacent to the specimen ends (run 3835). These microcracks occur as both grain boundary openings and transgranular microcracks (Figure 5b). There are no apparent differences in length and width between grain boundary cracks and the transgranular cracks. Thin lenticular deformation twins are present in many grains. At 15% strain, the abundance of deformation twins increases substantially and gentle bending of twins in some grains provides evidence for the operation of dislocation glide. The microcrack distribution is now very heterogeneous with strain being localized along a shear band that is inclined at about 30° to the maximum shortening direction (run 3836). Within this 1 mm wide band, the calcite grains are intensely fragmented by anastomosing networks of grain boundary and transgranular cracks (Figure 5c). Distinct en echelon zones of fine-grained comminution products, up to 4 mm long and 200 μm wide, are also present. The microfracture density decreases abruptly away from the margins of the shear band, so that about 1 mm from the shear band a fairly constant background fracture density, as recorded in Table 2, is present.

At 50 MPa effective pressure and strains of 12% and 15%, the grain boundary regions of many grains become intensely fragmented. Transgranular cracks are shorter than at 30 MPa effective pressure and their length increases only slightly with strain, while their abundance doubles between strains of 4% and 15% (Table 2). Deformation twins and lattice bending are also well-developed, especially at the higher strains.

At effective pressures of 100 MPa and 200 MPa, microstructural evidence for intracrystalline plasticity is much more pronounced than at lower effective pressures. Many grains already show at least two sets of deformation twins at 7.6% strain. At 17% strain, twins are more abundant and more strongly bent. The transgranular microcracks have substantially lower abundance and length than at lower effective pressures (Table 2). They are commonly lenticular to wedge-shaped, with lower aspect ratios (length/width) than is typical for specimens deformed at lower effective pressures (Figure 5d). Many radiate from grain boundaries while others are localized along the boundaries of deformation twins. Intergranular dilation and sliding, especially within the more highly deformed shear bands, have produced irregular damage zones composed of finely comminuted calcite.

**HP-I calcite.** The undeformed synthetic HP-I calcite aggregate has a polygonal grain structure with arrays of isolated pores along grain edges or grain corners (Figure 5e). At effective pressures of 20 MPa and 50 MPa, deformation is concentrated in shear zones, away from which grain boundary microcracks are prominent (Figure 5f). These cracks usually have lengths comparable to the grain diameter (about 18 μm) and an average width about 1 μm. Deformation twins are abundant and very thin microcracks are visible along them. Some short, wedge-shaped cracks are observed inside grains and seem to have initiated either from grain boundaries or from the ends of twins.

In the specimens deformed at an effective pressure of 100 MPa, two conjugate brittle shear zones occur at very high angle (>60°) to the maximum compression direction. Flattened grain shapes have developed.

## Discussion

### General Aspects

Figures 3b, 3c and 4b show that at a given strain, the porosity and the permeability both tend to increase more at smaller effective pressures but that except at small strains the permeability increases less markedly with strain than does the porosity. Figure 6 shows the relationship between permeability ($k$) and connected porosity ($\phi_c$), the latter being derived from data in Figures 3b and 4b by adding to the measured apparent connected porosity changes the small initial connected porosity (taken from *Fischer and Paterson* [1989, Table 1] for Carrara marble and assumed zero for HP-I). It is evident that this relationship is strongly dependent on the effective pressure, and that, in the one experiment for which data are available, the relationship for the fine-grained synthetic aggregate is similar to that for the marble. At 30 MPa effective pressure, there is at first a dramatic increase in permeability (up to 2 orders of magnitude) associated with only a small increase in connected porosity, but there is a less marked increase in permeability as the porosity is increased substantially during further deformation. At higher effective pressures, the initial large jump in permeability with connected porosity is less marked or absent.

The strong influence of effective pressure on permeability observed in our experiments is generally consistent with the results of *Fischer and Paterson* [1992] although their permeability experiments were of a different nature, in that they examined effective pressure dependence at given strain rather than strain dependence at given effective pressure, as in our study. However, at a given effective pressure, the permeability of undeformed Carrara marble in our experiments is about 1 to 1.5 orders of magnitude higher than that of *Fischer and Paterson* [1992]. The difference is probably caused by specimen anisotropy and, more importantly, by different experimental procedures. Unlike in our experiments where a designated effective pressure was maintained during pressurization, all specimens of *Fischer and Paterson* [1992] were first subject to a confining pressure of 300 MPa before being taken to a designated effective pressure. This procedure will have resulted in nonrecoverable crushing of pre-existing pores.

The storativity is higher in specimens strained at the lowest effective pressure, 30 MPa (Figure 3d), but the results from 50 to 200 MPa are more or less indistinguishable within the rather large scatter. Figure 7, which illustrates the relationships between storativity and connected porosity, shows that, as would be expected, the storativity generally increases as the porosity increases, possibly somewhat more strongly than linearly. There is also a distinct trend for lower storativity at 50 MPa effective pressure than at either 30 or 100 MPa. The results for 150 and 200 MPa are too few and scattered to show any consistent trends or to be distinguished from the results at 100 MPa.

The microscopical observations are consistent with the large initial jump in permeability with deformation at low effective pressures being due to the formation of connected

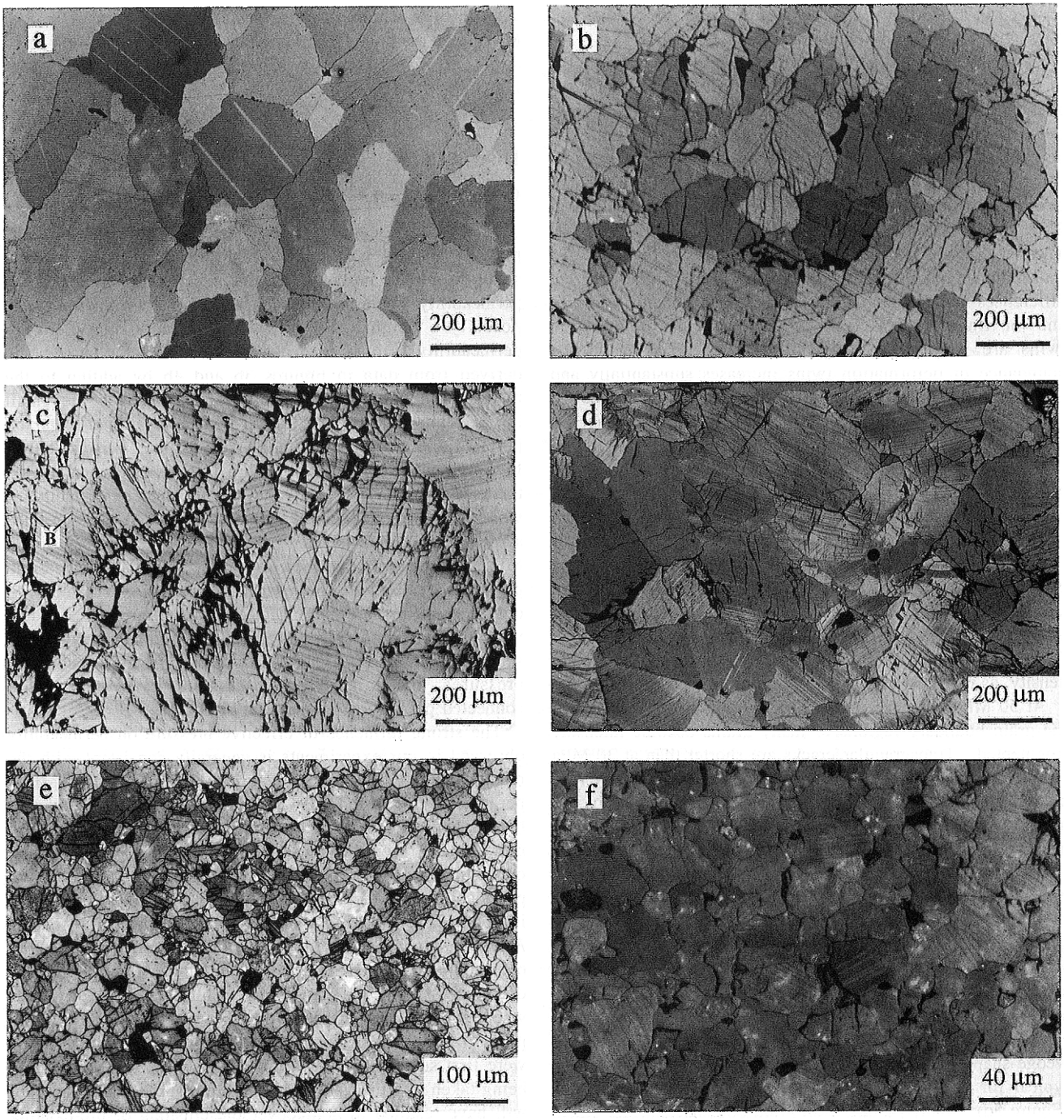


**Figure 5.** Microstructures on polished sections under reflected plane-polarized light. (a) Undeformed Carrara marble. (b) Carrara marble deformed 2.5% at room temperature and an effective pressure of 30 MPa (specimen 3835). Long and thin transgranular and grain boundary cracks are subparallel to the shortening direction (vertical). (c) Carrara marble deformed 15% at room temperature and an effective pressure of 30 MPa (specimen 3836). Shortening direction is vertical. Damage zones tend to be developed along some grain boundary regions. Debris and very fine crush products are present within the damage zones. Transgranular cracks are longer, wider, and more closely spaced than those in the less deformed specimen. Some transgranular cracks have formed parallel to cleavages and deformation twins. (d) Carrara marble deformed 17% at room temperature and an effective pressure of 200 MPa (specimen 3901). Shortening direction is vertical. Transgranular cracks are shorter than in specimens deformed to comparable strain at lower effective pressures. Deformation twins and lattice bending are more widespread than at low effective pressures. (e) Undeformed HP-I synthetic calcite aggregates with polygonal grain structure. (f) HP-I deformed 12% at room temperature and an effective pressure of 50 MPa (specimen 3827). Short grain boundary cracks are dominant and some grains are elongate perpendicular to the maximum shortening direction (which is vertical).

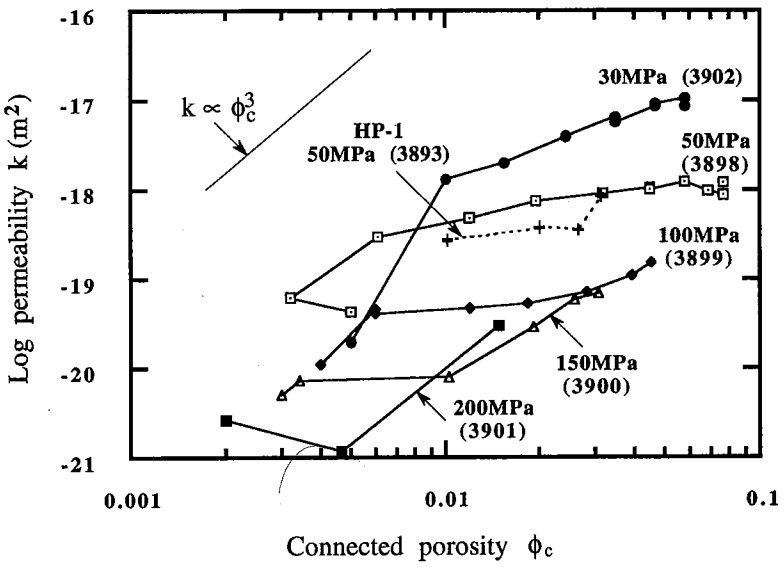


**Figure 6.** Relationship between permeability and connected porosity during deformation of Carrara marble (solid lines) and HP-I calcite aggregates (dashed line).

networks of microcracks. At higher strains at the low effective pressures, much of the porosity increase appears to be due to formation of shear zones and damage zones in grain boundary regions, in which the pores are on a very fine scale (crush products) and presumably do not augment the permeability appreciably in spite of the further increase in connected porosity. At higher effective pressures, the propagation of microcracks seems to be inhibited. Presumably, the strain is now achieved to a higher degree by crystal plasticity, so that higher strains are required to establish increased connectivity in the microcrack structure in order to produce an increase in permeability.

## Model Analysis

Since the microstructural observations indicate that the observed increases in permeability are accompanied by a proliferation of microcracking, we might approach the analysis of the measurements of permeability and storativity in terms of a model of penny-shaped microcracks of aperture $c$, using the percolation theory approach of *Dienes* [1982] and *Gueguen and Dienes* [1989], assuming a random orientation of equisized cracks. They predict the permeability to be

$$k = \frac{1}{30} f \phi c^2 \tag{1}$$

where $\phi$ is the total porosity and $f$ is the connectivity factor, equal to the fraction of cracks that are connected in a continuous path through the specimen. It follows from the definition of $f$ that $f\phi = \phi_c$, where $\phi_c$ is the connected porosity, and so

$$k = \frac{1}{30} \phi_c c^2 \quad \text{or} \quad c = 5.5\sqrt{\frac{k}{\phi_c}} \; . \tag{2}$$

The model apertures derived using (2) are plotted in Figure 8a.

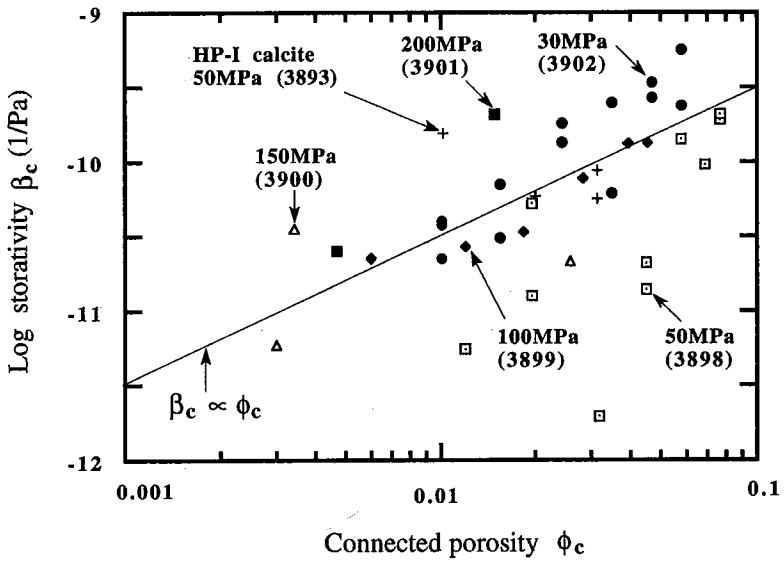


**Figure 7.** Relationship between storativity and connected porosity during deformation of Carrara marble at room temperature and effective pressures of 30 - 200 MPa.

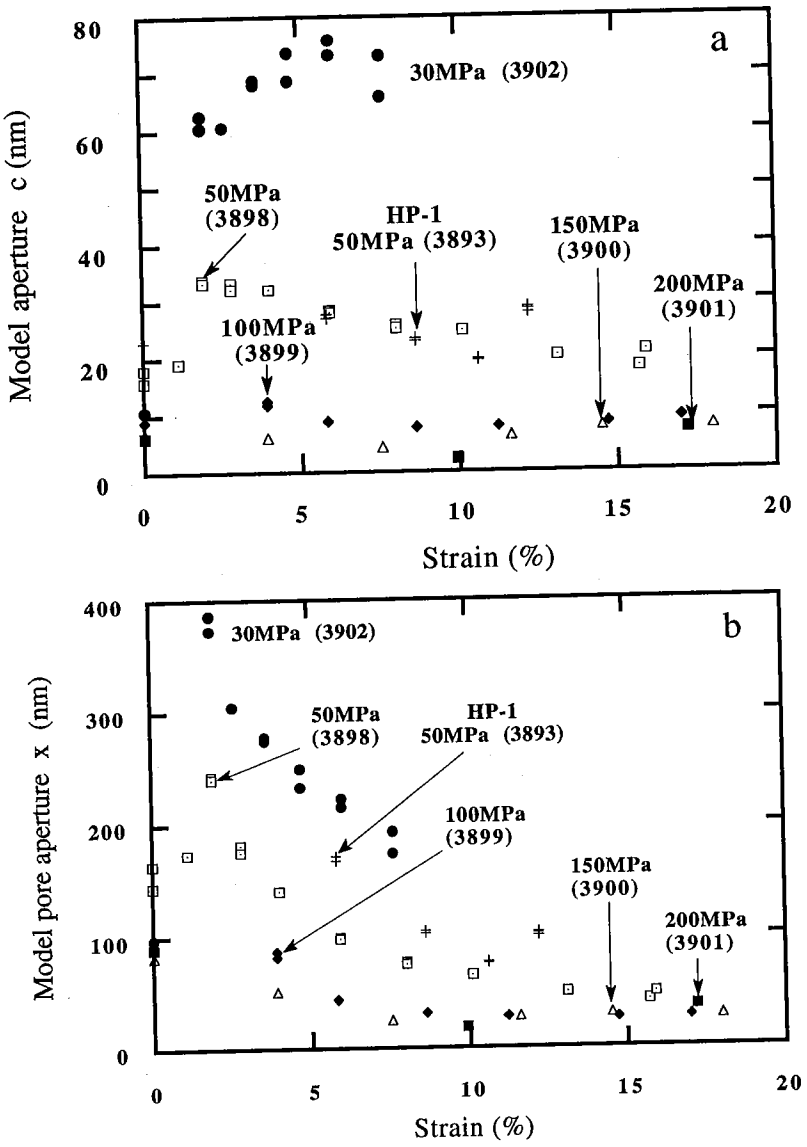


**Figure 8.** Changes in model microcrack aperture ($c$ and $x$) with strain. (a) Percolation theory approach: $c \approx 5.5\sqrt{k}/\sqrt{\phi_c}$. (b) Equivalent channel approach: $x \approx 3.5\sqrt{k}/\phi_c$.

If, alternatively, we use the equivalent channel approach [*Paterson*, 1983; *Walsh and Brace*, 1984], in which the porosity is implicitly assumed to be all connected, the permeability $k$ is predicted to be

$$k = \frac{\phi_c x^2}{12T} \tag{3}$$

where $T = (\ell_e / \ell)^2$ is the tortuosity factor ($\ell_e$ being the effective channel length for a distance $\ell$ in the direction of macroscopic flow) and $x$ is the channel aperture. Now introducing Archie's Law in the equivalent form $T = \phi^{1-m}$ into (3), as done by *Fischer and Paterson* [1992], we obtain the expression

$$x = 3.5 \frac{\sqrt{k}}{\phi_c} \tag{4}$$

The model apertures obtained using (4) are shown in Figure 8b. The two approaches are only equivalent if the tortuosity $T$ is constant and equal to 2.5, independent of the porosity. However, such a situation seems oversimplistic and so we subjectively prefer the more empirically-based equivalent channel model which envisages a variation of tortuosity with the porosity. This analysis, especially the trends shown in Figure 8b, indicates that the dramatic rise in permeability at small strains in the experiment at 30 MPa effective pressure is associated with the introduction of a relatively small number of new microcracks of relatively large aperture. With further deformation and, presumably, proliferation of the microcracking, the average aperture appears to decrease again. At higher effective pressures, the changes in model crack aperture are less marked.

In principle, the measurements of storativity, $\beta_c$, give information about the elastic properties of the pore space, through the relation of *Brace et al.* [1968]:

$$\beta_c = \phi_c (\beta_f - \beta_m) + (\beta_b - \beta_m) \tag{5}$$

where $\beta_f$ is the compressibility of the pore fluid, $\beta_b$ the bulk compressibility of the specimen, and $\beta_m$ the compressibility of the constituent mineral grains ($1.314 \times 10^{-11}$ Pa$^{-1}$ for calcite

at room temperature and 300 MPa [*Carmichael*, 1984]). Using the theory of elasticity of porous bodies, (5) can be inverted [*Fischer and Paterson*, 1992; *Zhang et al.*, this issue] to give an expression for the model aspect ratio of the pores,

$$\frac{a}{c} \approx 1 + \frac{\beta_f}{\beta_m}\left(\frac{\beta_c}{\phi_c \beta_f} - 1\right). \quad (6)$$

It is also argued by *Fischer and Paterson* [1992], from a consideration of the likely uncertainties in the measurements (their procedures are similar to those used here), that (6) can only give meaningful results if $\beta_c/\phi_c\beta_f > 2$. Using this selection criterion, the results for *a/c* are plotted in Figure 9. Although these results must be regarded as being approximate, they suggest that the model crack aspect ratio increases with increasing deformation at an effective pressure of 30 MPa but not at effective pressures of 50 and 100 MPa.

### Geological Implications of Microcrack Permeability

Although many separate porosity and permeability measurements have been reported in the last 20 years, there is a general lack of simultaneous measurements of permeability and porosity in the same experiment, especially during deformation [see *Zoback and Byerlee*, 1975; *Peach*, 1991; *Stormont and Daemen*, 1992). In many cases the permeability is inferred from connected porosity based on the equivalent channel model [e.g., *Heard and Page*, 1982; *Vaughan et al.*,1986; *Bickle and McKenzie*, 1987; *Thompson and Connolly*, 1990]. Our experiments on calcite rocks and previous studies on rock salt [*Peach*, 1991; *Stormont and Daemen*, 1992] indicate that the cubic law between permeability and total porosity does not hold near the threshold porosity and that permeability does not always increase with increasing deformation. Our experiments indicate that permeability can increase by up to 2 orders of magnitude with strains as low as 2% at low effective pressures. Because the pore fluid pressure can be near to the lithostatic pressure during regional deformation in many metamorphic terranes [*Etheridge et al.*, 1983, 1984; *Wood and Walther*, 1986; *Nur and Walder*, 1990], grain-scale microcracking could lead to at least transiently high permeabilities and associated high fluid flux. The experimental results demonstrate the importance of microcrack permeability for controlling fluid flow during crustal deformation and metamorphism, as suggested by *Cox and Etheridge* [1989] on the basis of field studies.

The room temperature deformation of calcite aggregates and the attendant changes in fluid transport properties involve both intercrystalline plasticity and microcracking [*Edmond and Paterson*, 1972; *Fredrich et al.*, 1989; *Evans et al.*, 1990]. Similar micromechanics are expected to control the behavior of silicates minerals near the brittle-plastic transition at mid to lower crustal levels. Thus the fluid transport properties in the Earth's mid to lower crust may be substantially influenced by both active deformation and variations in pore fluid. In particular, our experimental results highlight the potential importance of low strain deformation events and strain localization in controlling the timing and architecture of fluid migration through the Earth's crust.

## Conclusions

Changes in permeability and the apparent connected porosity of calcite aggregates have been measured during room temperature deformation as a function of strain and effective pressure. The porosity and permeability measurements led to the following results.

1. The apparent connected porosity increases continuously after compaction with increasing plastic strain and decreasing effective pressure. Permeability development is also sensitively dependent on effective pressure and strain. At effective pressures less than 50 MPa, the permeability increases by 1 to 2 orders of magnitude with an initial 2-5% strain and an accompanying increase of 0.005-0.01 in apparent connected porosity. The permeability increased only slightly with further shortening up to 18% and increase in apparent connected porosity up to 0.08. At effective pressures of 150 to 200 MPa, the permeability did not increase substantially until specimens were shortened by about 8%.

2. Microstructural analysis indicates that increases in permeability during deformation are associated with the formation of microcracks and the establishment of interconnection between them. In Carrara marble specimens

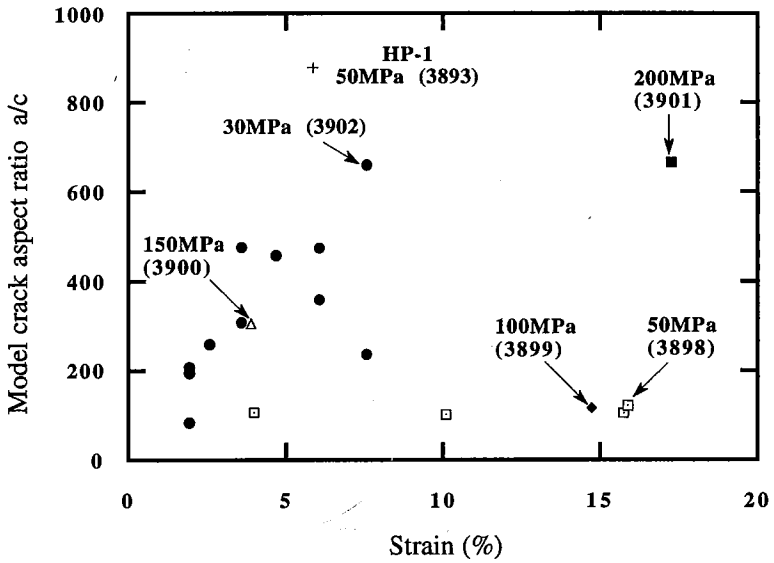


**Figure 9.** Changes in model microcrack aspect ratio *a/c* with strain.

deformed at low effective pressures, long and thin transgranular and grain boundary cracks are dominant. Increases in apparent connected porosity are achieved mainly by the broadening of damage zones around grain boundary regions and by the broadening of conjugate dilatant shear zones within specimens. In specimens deformed at high effective pressures, microcracks tend to be shorter and wider than those formed at lower effective pressures. In the fine-grained hot-pressed synthetic specimens, the permeability increase is mainly due to the formation of relatively low aspect ratio (blunt) cracks along grain boundaries.

**Acknowledgments.** During this research, Shuqing Zhang was a recipient of an Australian National University Ph.D. scholarship and a postgraduate scholarship from the K. C. Wong Education Foundation (Hong Kong) Ltd. Stephen Cox acknowledges the support of an Australian Research Council Senior Research Fellowship. The authors thank Ian Jackson and George Fischer for their advice on techniques and analysis of experimental results. Many thanks are due to Graeme Horwood for the maintenance of the high-pressure apparatus.

## References

Beach, A., Retrogressive metamorphic processes in shear zones with special reference to the Lewisian complex, *J. Struct. Geol.*, *2*, 257-263, 1980.

Bickle, M. J., and D. McKenzie, The transport of heat and matter by fluids during metamorphism, *Contrib. Mineral. Petrol.*, *95*, 384-392,1987.

Brace, W. F., J. B. Walsh, and W. T. Frangos, Permeability of granite under high pressure, *J. Geophys. Res.*, *73*, 2225-2236, 1968.

Brantley, S. L., The effect of fluid chemistry on quartz microcrack lifetimes, *Earth Planet. Sci. Lett.*, *113*, 145-156, 1992.

Brantley, S. L., B. Evans, S. H. Hickman, and D. A. Crerar, Healing of microcracks in quartz: implications for fluid flow, *Geology*, *18*, 136-139, 1990.

Carmichael, R. S., *Handbook of Physical Properties of Rocks, vol.3*, pp.111, CRC Press, Boca Raton, Fla., 1984.

Cox, S. F., and M. A. Etheridge, Coupled grain-scale dilatancy and mass transfer during deformation at high fluid pressures: Examples from Mount Lyell, Tasmania, *J. Struct. Geol.*, *11*, 147-162, 1989.

Cox, S. F., M. A. Etheridge, and V. J. Wall, The role of fluids in syntectonic mass transport, and the localization of metamorphic vein-type ore deposits, *Ore Geol. Rev.*, *2*, 65-86, 1987.

Dienes, J. K., Permeability, percolation and statistical crack mechanics, in *Issues in Rock Mechanics*, edited by R. E. Goodman and F. E. Heuze, pp.86-94, American Institute of Mining, Metallurgical and Petroleum Engineering, New York, 1982.

Edmond, J. M., and M. S. Paterson, Volume change during the deformation of rocks at high pressures, *Int. J. Rock Mech. Min. Sci.*, *9*, 161-182, 1972.

Etheridge, M. A., V. J. Wall, and R. H. Vernon, The role of the fluid phase during regional metamorphism and deformation, *J. Metamorph. Geol.*, *1*, 205-226, 1983.

Etheridge, M. A., V. J. Wall, S. F. Cox, and R. H. Vernon, High fluid pressure during regional metamorphism and deformation: Implications for mass transport and deformation mechanisms, *J. Geophys. Res.*, *89*, 4344-4358, 1984.

Evans, B., J. T. Fredrich, and T. F. Wong, The brittle-ductile transition in rocks: recent experimental and theoretical progress, in *The Brittle-Ductile Transition in Rocks*, edited by A. Duba, W. Durham, J. Handin, and H. F. Wang, Geophys. monogr. Ser., vol.56, pp.1-20, AGU, Washington, D. C., 1990.

Fischer, G. J., The determination of permeability and storage capacity: pore pressure oscillation method, in *Fault Mechanics and Transport Properties of Rocks*, edited by B. Evans and T. F. Wong, pp.187-211, Academic, San Diego, Calif., 1992.

Fischer, G. J., and M. S. Paterson, Permeability and storage capacity during deformation at elevated temperatures (abstract), *EOS, Trans. AGU*, *69*, 484, 1988.

Fischer, G. J., and M. S. Paterson, Dilatancy during rock deformation at high temperatures and pressures, *J. Geophys. Res.*, *94*, 17,607-17,617, 1989.

Fischer, G. J. and M. S. Paterson, Measurements of permeability and storage capacity in rocks during deformation at high temperature and pressure, in *Fault Mechanics and Transport Properties of Rocks*, edited by B. Evans and T. F. Wong, pp.213-252, Academic, San Diego, Calif., 1992.

Fredrich, J. T., B. Evans, and T. F. Wong, Micromechanics of the brittle to plastic transition in Carrara marble, *J. Geophys. Res.*, *94*, 4129-4145, 1989.

Fredrich, J. T., B. Evans, and T. F. Wong, Effect of grain size on brittle and semibrittle strength: Implications for micromechanical modeling of failure in compression, *J. Geophys. Res.*, *95*, 10,907-10,920, 1990.

Gueguen, Y., and J. K. Dienes, Transport properties of rocks from statistics and percolation, *Math. Geol.*, *21*, 1-13, 1989.

Heard, H. C., Effect of large changes in strain rate in the experimental deformation of Yule Marble, *J. Geol.*, *71*, 162-195, 1963.

Heard, H. C., and L. Page, Elastic moduli, thermal expansion, and inferred permeability of two granites to 350°C and 55 megapascals, *J. Geophys. Res.*, *87*, 9340-9348, 1982.

Kerrich, R., Fluid transport in lineaments, *Philos. Trans. R. Soc. London A*, *317*, 219-251, 1986.

Kranz, R. L., J. S. Saltzman, and J. D. Blacic, Hydraulic diffusivity measurements on laboratory rock samples using an oscillating pore pressure method, *Int. J. Rock Mech. Min. Sci. Geomech. Abstr.*, *27*, 345-352, 1990.

Lee, V. W., S. J. Mackwell, and S. L. Brantley, The effect of fluid chemistry on wetting textures in Novaculite, *J. Geophys. Res.*, *96*, 10,023- 10,037, 1991.

McCaig, A. M., Deep fluid circulation in fault zones, *Geology*, *16*, 867-870, 1988.

Moore, J. C., and P. Vrolijk, Fluids in accretionary prisms, *Rev. Geophys.*, *30*, 113-135, 1992.

Nur, A., and J. Walder, Time-dependent hydraulics of the Earth's crust, in *The Role of Fluid in Crustal Processes, Studies in Geophysics*, pp.113-127, National Academy Press, Washington, D. C., 1990.

Olsson, W.A., and S. S. Peng, Microcrack nucleation in marble, *Int. J. Rock Mech. Min. Sci. Geomech. Abstr.*, *13*, 53-59, 1976.

Paterson, M. S., Secondary changes of length with pressure in experimentally deformed rocks, *Proc. R. Soc. London A*, *271*, 57-87, 1963.

Paterson, M. S., A high-pressure, high-temperature apparatus for rock deformation, *Int. J. Rock Mech. Min. Sci.*, *7*, 517-526, 1970.

Paterson, M. S., The equivalent channel model for permeability and resistivity in fluid-saturated rock -- A re-appraisal, *Mech. Mater.*, *2*, 345-352, 1983.

Peach, C. J., Influence of deformation on the fluid transport properties of salt rocks, *Geologica Ultraiectina, No.77*, Instituut voor Aardwetenschappen der Rijksuniversiteit Utrecht, 238pp., 1991.

Rutter, E. H., The influence of temperature, strain rate and interstitial water in the experimental deformation of calcite rocks, *Tectonophysics*, *22*, 311-334, 1974.

Rutter, E. H., and K. H. Brodie, The permeation of water into hydrating shear zones, in *Advances in Physical Geochemistry, vol.5*, edited by Thompson, A. B. and Rubie, D. C., pp.242-250, Springer-Verlag, New York, 1985.

Scholz, C. H., Microfracturing and inelastic deformation of rock in compression, *J. Geophys. Res.*, *73*, 1417-1432, 1968.

Sibson, R. H., F. Robert, and K. H. Poulsen, High-angle reverse faults, fluid-pressure cycling, and mesothermal gold-quartz deposits, *Geology*, *16*, 551-555, 1988.

Smith, D. L., and B. Evans, Diffusional crack healing in quartz, *J. Geophys. Res.*, *89*, 4125-4135, 1984.

Stormont, J. C., and J. K. Daemen, Laboratory study of gas permeability

changes in rock salt during deformation, *Int. J. Rock Mech. Min. Sci. Geomech. Abstr.*, *29*, 325-342, 1992.

Thompson, A. B., and J. A. D. Connolly, Metamorphic fluids and anomalous porosities in the lower crust, *Tectonophysics*, *182*, 47-55, 1990.

Vaughan, P. J., D. E. Moore, C. A. Morrow, and J. D. Byerlee, Role of cracks in progressive permeability reduction during flow of heated aqueous fluids through granite, *J. Geophys. Res.*, *91*, 7517-7530, 1986.

Walsh, J. B., and W. F. Brace, The effect of pressure on porosity and the transport properties of rock, *J. Geophys. Res.*, *89*, 9425-9431, 1984.

Wood, B. J., and J. V. Walther, Fluid flow during metamorphism and its implications for fluid-rock ratios, in *Fluid-rock Interactions During Metamorphism, vol.5*, edited by J. V. Walther and B. J. Wood, pp.89-108, Springer-Verlag, New York, 1986.

Zhang, S., M. S. Paterson, and S. F. Cox, Porosity and permeability evolution during hot isostatic pressing of calcite aggregates, *J. Geophys. Res.*, this issue.

Zoback, M. D., and J. D. Byerlee, Permeability and effective stress, *Pet. Geol.*, *59*, 154-158, 1975.

---

Stephen F. Cox and Mervyn S. Paterson, Research School of Earth Sciences, Australian National University, Canberra, ACT 0200, Australia.

Shuqing Zhang, Department of Geology and Geophysics, University of Minnesota, 310 Pillsbury Drive S.E., Minneapolis, MN 55455. (e-mail: zhang038@maroon.tc.umn.edu).

(Received May 24, 1993; revised December 27, 1993;
accepted March 7, 1994)